Magnetic Resonance in Medicine 53:1468–1473 (2005)

Spiral Balanced Steady-State Free Precession Cardiac Imaging

Krishna S. Nayak,[1,2]* Brian A. Hargreaves,[1] Bob S. Hu,[1,3] Dwight G. Nishimura,[1] John M. Pauly,[1] and Craig H. Meyer[1,4]

Balanced steady-state free precession (SSFP) sequences are useful in cardiac imaging because they achieve high signal efficiency and excellent blood–myocardium contrast. Spiral imaging enables the efficient acquisition of cardiac images with reduced flow and motion artifacts. Balanced SSFP has been combined with spiral imaging for real-time interactive cardiac MRI. New features of this method to enable scanning in a clinical setting include short, first-moment nulled spiral trajectories and interactive control over the spatial location of banding artifacts (SSFP-specific signal variations). The feasibility of spiral balanced SSFP cardiac imaging at 1.5 T is demonstrated. In observations from over 40 volunteer and patient studies, spiral balanced SSFP imaging shows significantly improved contrast compared to spiral gradient-spoiled imaging, producing better visualization of cardiac function, improved localization, and reduced flow artifacts from blood. Magn Reson Med 53:1468–1473, 2005. © 2005 Wiley-Liss, Inc.

Key words: steady-state free precession; spiral MRI; cardiac imaging; flow artifacts; gradient design

Real-time spiral MRI has proven to be clinically useful for evaluating cardiac function (1), visualizing cardiac flow (2), and localizing scan planes for coronary imaging (3). Spiral acquisitions provide an efficient acquisition of *k*-space that has good motion properties as well as some SNR benefits (4).

Balanced steady-state free precession (SSFP) sequences (also known as True-FISP, FIESTA, or balanced FFE) are extremely useful in cardiac imaging because they provide high SNR and excellent blood–myocardium contrast. Contrast is based on T_2/T_1 resulting in high blood signal (independent of inflow) and high blood–myocardium contrast. Their main limitations are sensitivity to off-resonance, typically requiring an imaging TR of 2 to 6 ms (at 1.5 T), and transient artifacts observed when imaging a new volume or when objects move into or out of the imaging volume.

[1]Magnetic Resonance Systems Research Laboratory, Department of Electrical Engineering, Stanford University, Stanford, California, USA.

[2]Magnetic Resonance Engineering Laboratory, Department of Electrical Engineering, University of Southern California, Los Angeles, California, USA.

[3]Division of Cardiovascular Medicine, Palo Alto Medical Foundation, Palo Alto, California, USA.

[4]Department of Biomedical Engineering, University of Virginia, Charlottesville, Virginia, USA.

Grant sponsor: National Institutes of Health; Grant numbers: R01-HL/067161 and R01-HL/074332; Grant sponsor: GE Healthcare; Grant sponsor: The Whitaker Foundation.

*Correspondence to: Krishna S. Nayak, Electrical Engineering–Systems, 3740 McClintock Avenue, EEB 406, University of Southern California, Los Angeles, CA 90089-2564, USA. E-mail: knayak@usc.edu

Received 27 August 2004; revised 4 January 2005; accepted 6 January 2005.

DOI 10.1002/mrm.20489

Published online in Wiley InterScience (www.interscience.wiley.com).

We have developed a real-time interactive pulse sequence that combines the imaging efficiency and real-time capabilities of spiral acquisitions with the SNR and contrast benefits of balanced SSFP. Key developments include the introduction of first-moment nulling to mitigate in-plane flow artifacts and implementation within a real-time interactive framework to enable real-time adjustment of the center frequency (and thus the balanced SSFP signal profile). Design specifications, in vivo results, and observations are presented.

THEORY

Balanced SSFP sequences, as well as their signal behavior, have been studied since well before MRI itself (5). More recently, balanced SSFP has been enabled by advances in gradient amplifier strength and speed (6). In balanced SSFP, the steady-state signal amplitude varies significantly with resonant frequency as is well described by Scheffler and Lehnhardt (7). The magnitude signal consists of high-signal "passbands" separated by signal nulls that repeat at a frequency spacing of 1/TR, where TR is the sequence repetition time. To reduce sensitivity to off-resonance effects, it is essential to keep a reasonable passband bandwidth and thus to keep the TR short.

To maintain the high-SNR-efficiency steady state, the effect of all gradients over a sequence repetition would ideally be zero. For stationary tissues, this means that the gradient area must be zero between excitation pulses. For moving spins, this also means that higher-order gradient moments should also be zero between excitation pulses. Rewinding the gradient zeroth and first moments is sufficient if velocities can be assumed to be constant during a TR.

METHOD

Experimental Setup

Studies were performed on two GE Signa 1.5-T LX systems, with gradients capable of 40 mT/m amplitude and 150 T/m/s slew rate and receivers supporting 4-μs sampling (±125 kHz). A 5-inch surface coil was used for signal reception in all studies. The institutional review board of Stanford University approved the imaging protocols. Subjects were screened for magnetic resonance imaging risk factors and provided informed consent in accordance with institutional policy.

Sequence designs were optimized for this scanner configuration, and in vivo results were acquired on the above-stated hardware. Generic sequence design methods are described in the following sections.

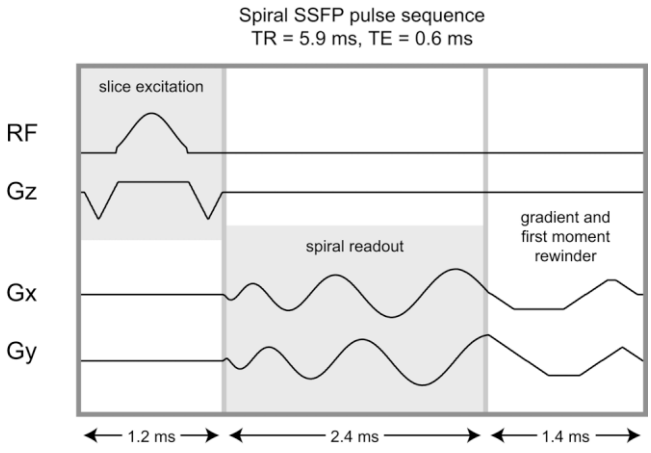

FIG. 1. 2D spiral SSFP sequence used in the in vivo studies. Each TR consisted of a 1.2-ms excitation (640-μs RF) followed by 2.4-ms spiral readout and 1.4-ms refocusing. The refocusing nulls the zeroth and first moments of the gradient waveform for consistent signal in the presence of in-plane flow. Due to practical limitations, there was 0.9 ms of dead time for each TR, which may be eliminated with a more optimized implementation.

Gradient Design Techniques

Spiral readouts were designed using optimal design techniques and numerical approaches (software available at http://www-mrsrl.stanford.edu/~brian/vdspiral/). Perhaps the most important element of the pulse sequence design was the design of the spiral *k*-space rewinder, which returns the spiral scan to the *k*-space origin. Rewinding the zeroth moment (or area) is necessary to maintain balanced SSFP coherence. However, because of the significant in-plane motion and flow in cardiac imaging, moment nulling between RF pulses is also needed to prevent phase-related flow artifacts.

It is possible to first add a zeroth-moment rewinder and then follow that with a bipolar gradient to compensate the first moment. However, this would prolong the TR, increasing the sensitivity to banding artifacts and increasing the sensitivity to higher-order motion as well as reducing SNR efficiency. A better solution is to design the *k*-space rewinder so that it simultaneously compensates the zeroth and first moments.

The 2D spiral gradients must be "freely rotatable," meaning that they can be rotated to any angle without violating gradient amplitude or slew-rate limits. The in-plane gradients are referred to as *x* and *y*. A quick, but suboptimal method of designing the rewinder gradients is to choose some angle ϕ and limit the *x* and *y* gradients (amplitude and slew-rates) to cos ϕ and sin ϕ times the physical limits. This allows independent design of both *x* and *y* waveforms, which has been solved previously (8) and is shown in Fig. 1. The design can be repeated for different ϕ, say 30, 45, and 60°, and the shortest duration design used. Although this is relatively simple, it is significantly slower than the methods described below.

One method for designing shorter rewinders is to first assume that gradient waveforms will take a certain overall shape and then to use moment constraints to find the parameters of this shape. In particular, we make the following assumptions about the shape of the rewinders: (1) the rewinders will include triangles of alternating polarity, (2) the vector slew rate magnitude ($|d\bar{G}/dt|$) should be at the maximum allowed rate to minimize the width of the triangles, and (3) the *x* and *y* rewinders that result will be about the same length.

Figure 2 shows the assumed shape of the rewinders and defines the variables used in the design. Prior to designing the rewinders, the spiral gradients are rotated so that the *y* gradient ends with zero amplitude. This results in no loss of generality and simplifies the design. To make the zeroth and first moments of the combination of the spiral gradient and rewinder equal to zero, the moments of the rewinder must be equal to the negative of the moments of the spiral readout gradient, using the same time origin.

Assume that the spiral gradients are of duration *T* and place the time origin at the end of the spiral readout gradients. With these assumptions, let the zeroth moment at the start of the rewinder be $M_0 = \int_{-T}^{0} G(t)dt$ and let the first moment be $M_1 = \int_{-T}^{0} t\,G(t)dt$. Also, let *S* be the maximum allowed rotatable slew rate, defined as $1/\sqrt{2}$

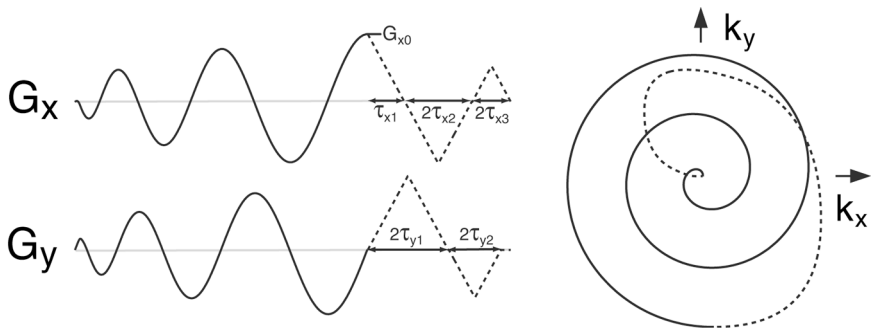

FIG. 2. Spiral SSFP gradient waveforms (left) with a *k*-space rewinder that simultaneously nulls the zeroth and first gradient moments and corresponding *k*-space trajectorory (right) including the rewinder. The solid line is the spiral readout, and the dashed line is the rewinder. Variable definitions for the gradient rewinder design are labeled. The spiral readout gradients are rotated prior to the rewinder design so that G_y ends at zero amplitude to simplify the design. The time origin is chosen to be the start of the rewinder. The widths of the rewinder gradient lobes are determined by solving Eqs. [1–4].

times the maximum gradient amplitude divided by the minimum rise time to that amplitude.

Once the design problem is constrained in this manner, it is straightforward to calculate the moments of the rewinders. For the initial G_x down ramp, $M_0 = G_{x0}\,\tau_{x1}/2$ and $M_1 = G_{x0}\,\tau_{x1}^2/6$. For a triangle of width 2τ centered at time t_0 with slew rate S, $M_0 = S\,\tau^2$ and $M_1 = S\,\tau^2\,t_0$. We then add up the appropriate components to calculate the total moment for each rewinder. To solve the moment-nulling problem for the x axis, we solve the following pair of simultaneous polynomial equations for τ_{x2} and τ_{x3}, with $\tau_{x1} = G_{x0}/S$:

$$-\frac{M_0}{S} = \frac{1}{2}\tau_{x1}^2 - \tau_{x2}^2 + \tau_{x3}^2 \quad [1]$$

$$-\frac{M_1}{S} = \frac{1}{6}\tau_{x1}^3 - \tau_{x2}^2(\tau_{x1} + \tau_{x2}) + \tau_{x3}^2(\tau_{x1} + 2\tau_{x2} + \tau_{x3}). \quad [2]$$

For the y axis, we solve the following pair of equations for τ_{y1} and τ_{y2}:

$$-\frac{M_0}{S} = \tau_{y1}^2 - \tau_{y2}^2 \quad [3]$$

$$-\frac{M_1}{S} = \tau_{y1}^3 - 2\tau_{y1}\tau_{y2}^2 - \tau_{y2}^3. \quad [4]$$

We then have all of the parameters needed to specify the rewinders (see Fig. 2). The X-gradient rewinder is determined by solving Eqs. [1] and [2], while the Y-gradient rewinder is determined by solving Eqs. [3] and [4]. Each pair of equations has four analytical solutions, but only one of those solutions is real and positive in each case. The solutions were found using the solve routine of the symbolic toolbox of Matlab (Mathworks, Inc., South Natick, MA, USA). The solutions are too long to include here, but are readily calculated polynomial expressions. Note that the equations can also be solved numerically using Matlab's fsolve routine and that the resulting solution matches the analytical solution for cases that we tested.

Newly developed time-optimal gradient rewinder design techniques can be used to further reduce the duration of the rewinding gradient (9). We compared the two rewinder design methods described above to the time-optimal solution, using the spiral parameters of Fig. 1. As shown in Fig. 3, the independent axis method results in a 1.41-ms rewinder; the triangle-wave method results in a 1.05-ms x-axis rewinder and a 0.94-ms y-axis rewinder; and the time-optimal solution results in a 1.03-ms rewinder. This comparison illustrates that the assumptions of the triangle-wave method yield very good, but not quite optimal, rewinders. The method is useful for scan-time gradient design because it has an analytical solution, whereas the time-optimal solution requires more powerful optimization software. For spiral scans with higher spatial resolutions that require larger rewinders, the method can be generalized to include trapezoidal elements.

Figure 4 compares a spiral SSFP image acquired with a conventional zeroth-moment rewinder with an image acquired using the flow-compensated gradients of Fig. 2. First moment nulling nearly eliminates the artifacts from in-plane flow.

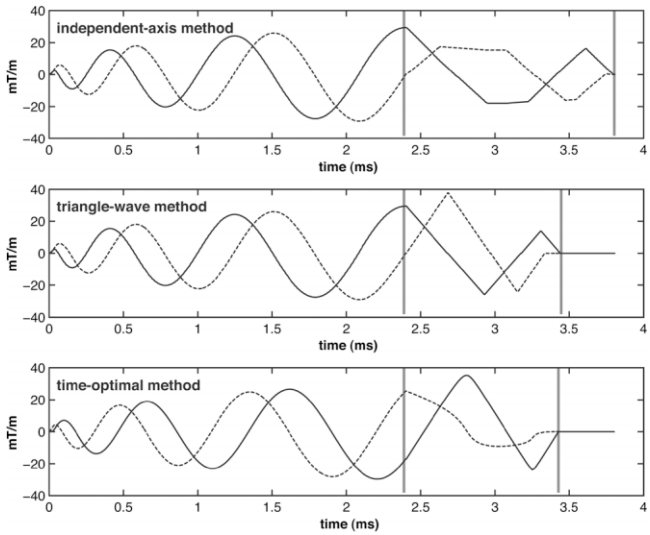

FIG. 3. Flow-compensated gradients designed using three different methods (solid = G_x, dashed = G_y). Top: The method of Fig. 1, which rewinds each axis independently. Middle: The triangle-wave method described by Eqs. [1–4]. Bottom: The time-optimal method (9). Gray lines indicate the beginning and end of the rewinders. The three methods result in progressively shorter rewinders of duration 1.41, 1.05, and 1.03 ms.

Pulse Sequence and Implementation

The imaging pulse sequence (shown in Fig. 1) consisted of a slice selective excitation followed by an interleaved spiral readout and gradient rewinders. The excitation pulse had a 640 μs RF, 1.2-ms slice-select gradient, 5-mm slice thickness, and nominal flip angle of 90°. Spiral interleaves had 2.4-ms duration and were followed by zeroth and first moment rewinders occupying 1.4 ms (independent-axis method). Twenty interleaves were used to achieve 1.8-mm in-plane resolution over a 20-cm FOV. The imaging TR was 5.9 ms, producing signal nulls spaced slightly over 180 Hz apart, and temporal resolution of 118 ms. Sliding window reconstruction was used to display 24 frames/s.

Pulse sequences and image reconstructions were implemented within a custom real-time imaging framework previously described by Kerr et al. (10). For SNR and contrast comparisons, real-time spiral gradient echo images were acquired using a spectral-spatial excitation and 16-ms spiral readouts as described previously (11) (spiral GRE, 30° flip, 29-ms TR, 4 interleaves, 1.8-mm resolution) to achieve the same temporal and spatial resolution as the spiral balanced SSFP sequence.

The literature, as well as our experience, suggests that at 1.5 T, most cardiac views can be achieved with less than 120 Hz of off-resonance across the heart (12). The TR of 5.9 ms and flip angle of 60–90° was used to maximize the readout duty-cycle and SNR, while maintaining a flat passband of at least 120 Hz.

In order to avoid banding artifacts on a per-slice basis, real-time phase-cycling was implemented. The applica-

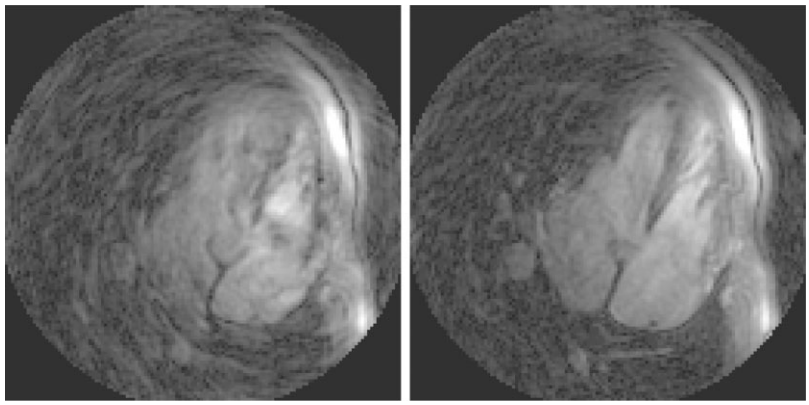

FIG. 4. Typical real-time spiral SSFP images acquired with (left) only zeroth moment refocusing and (right) zeroth and first moment refocusing. Notice that first moment nulling nearly eliminates the artifacts from in-plane flow.

tion of a constant phase increment to the RF and DAQ (13) waveforms produces a frequency shift in the SSFP signal profile. For example, with a phase increment of 0°, the signal nulls are at 0 and 166 Hz, and with a phase cycling increment of 180° (as is standard in balanced SSFP), the signal nulls are at ±83 Hz. A slider was added to the user interface to allow interactive, real-time adjustment of this phase increment and hence the passband center frequency.

The primary purpose was to ensure that on a slice-by-slice basis, images do not contain banding artifacts; however, rudimentary fat suppression could also be achieved by adjusting the phase cycling such that fat falls within a null in the signal profile, as shown in Fig. 5.

In order to achieve volumetric coverage within a breath-hold for LV function studies, trigger-based slice shifting was implemented in this system. As described previously (14), several slice loops may be acquired during consecutive R–R intervals in a breath-hold. In LV function studies, the phase increment was fixed for each set of slices; however, if needed, different phase increments could be preset for each slice. Images were segmented manually using Matlab.

RESULTS

Results are presented on an exemplary basis. A complete analysis of SNR, contrast-to-noise ratio (CNR), volumes, etc., was not performed.

Balanced SSFP versus GRE

Figure 6 contains sample still frames from short-axis and four-chamber views, comparing the image quality of real-time spiral SSFP with real-time spiral gradient echo (11) of identical resolution and scan time. In this representative example, blood–myocardium CNR in the short-axis view was 3.93 ± 2.92 using real-time spiral GRE and 22.82 ± 1.87 using real-time spiral balanced SSFP. The blood–myocardium contrast of SSFP was qualitatively found to be stable throughout the cardiac cycle and among different myocardial segments. The blood–myocardium contrast of GRE was highly dependent on both cardiac phase and myocardial segment. This, we expect, is due to inflow enhancement causing fluctuations in blood signal when using GRE. The GRE images also contained noticeable artifacts from in-plane flow (partial saturation), while balanced SSFP images were not adversely affected by such flow (15). Based on our experience scanning over 40 subjects, the balanced SSFP acquisitions achieve substantially higher blood–myocardium contrast (roughly 5×) and more consistent contrast, which allows for improved segmentation of the LV volume in short-axis views as well as improved visualization of chambers and valve leaflets in long-axis views.

LV Function

One application of real-time balanced SSFP cardiac imaging is the accurate assessment of ventricular volumes,

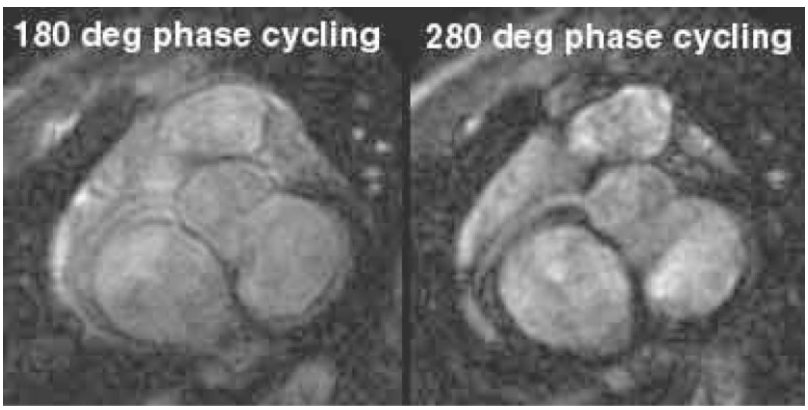

FIG. 5. Real-time spiral SSFP images of a right coronary artery with different phase-cycling increments. Rudimentary fat suppression can be achieved by adjusting phase increment (shifting the spectral profiles) such that fat (−220 Hz at 1.5 T) falls within an SSFP signal null.

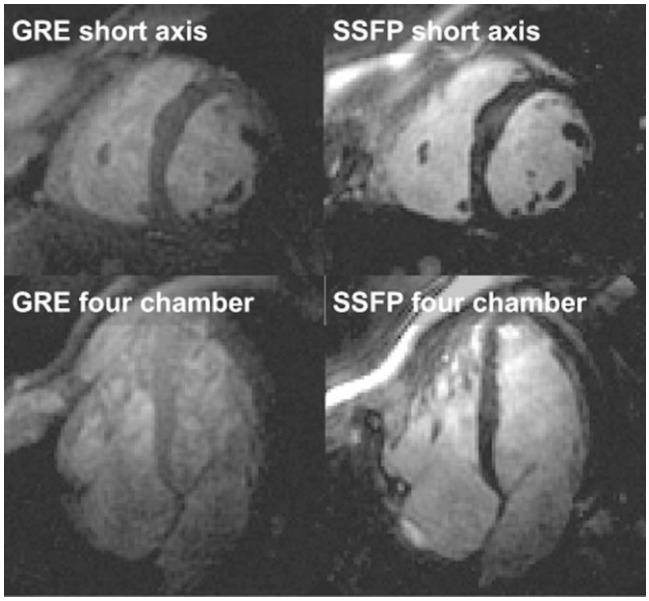

FIG. 6. Short-axis and four-chamber views acquired using real-time spiral (left) gradient echo and (right) SSFP MRI. SSFP's high blood–myocardium contrast and minimal in-plane flow artifacts enable easy segmentation of the LV volume.

mass, and function. Blood–myocardium contrast in conventional gradient echo imaging is predominantly from inflow enhancement, which can cause reduced contrast in areas of slow flow or in subjects with severe dysfunction. Balanced SSFP yields an intrinsic blood–myocardium contrast based on T_2/T_1 (see Fig. 6) and independent of inflow. Real-time spiral balanced SSFP's high temporal resolution permits the acquisition of volumetric time-resolved imaging in a single breath-hold using triggering (14). Figure 7 contains LV short-axis images from a patient with low ejection fraction (EF). End-diastolic and end-systolic frames from eight slices were acquired in a single 6-s breath-hold (100 bpm heart rate). These images were segmented to yield LV volumes, EF, and mass.

Note that spiral balanced SSFP provides excellent blood–myocardium contrast, enabling automated segmentation of the endocardial border. Automated segmentation of the outer LV border is still an area of research, due to the high signal from epicardial fat and other issues.

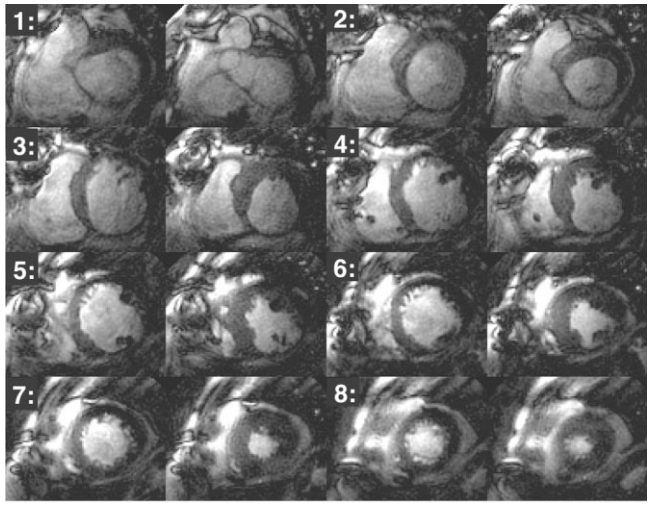

FIG. 7. Triggered spiral SSFP acquisition in an AS patient with low EF during one 6-s breath-hold. End-diastolic and end-systolic images are shown for each of eight short-axis slices spanning the LV. Based on manual segmentation: EDV = 181.4 mL, ESV = 108.8 mL, EF = 40%, LV mass = 199.1 g.

Flow Jets

Because all gradients are rewound, spins that have left the imaging slice after being excited can contribute image signal for many TR afterward (15). This produces a useful enhancement when visualizing fast flow, as seen in an aortic stenosis (AS) patient with a 4.7 m/s flow jet (Fig. 8). Excellent image quality, visualization of leaflets, and visualization of the flow jet are all achieved in real time using spiral balanced SSFP.

DISCUSSION

When changing the imaging slice, we observed a transient signal artifact that lasted about 150 to 210 ms. After implementing the standard "$\alpha/2$" pulse (16) on each new scan plane, or after pausing and restarting the scan, the duration of this transient did not noticeably change. This was only problematic during triggered LV function studies, where the trigger delay was set such that the transient occurred during the least critical portion of the cardiac cycle.

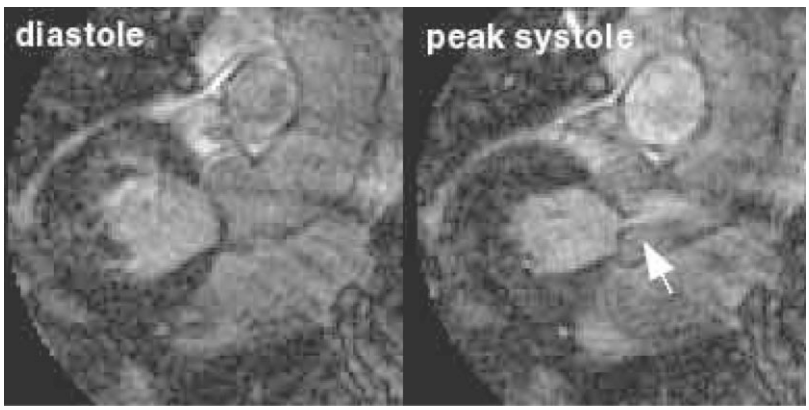

FIG. 8. Aortic stenosis visualized in real time using spiral SSFP: (left) valve closed in diastole, (right) barely open during peak systole.

Robust fat suppression remains a challenge in real-time SSFP imaging, especially for the localization and imaging of coronary arteries. Dixon-based techniques and linear-combination-based techniques are less attractive because they substantially increase scan time. Saturation-based schemes (17) will require repeated saturation and suffer from transient fat signal. Phase-based separation (18) is fast, but suffers from partial voluming, which can be significant in lower resolution real-time imaging.

Balanced SSFP, in general, provides excellent SNR. In combination with time-efficient spiral or echo-planar (19,20) readouts, this produces high-quality real-time images. Compared to EPI, we expect that spiral images will have better motion properties when there is motion during the acquisition window of a single image requiring multiple interleaves. Any off-resonance blurring should be insignificant in most cases because of the short readout duration.

CONCLUSIONS

We have demonstrated real-time interactive cardiac imaging using spiral balanced SSFP. The resulting images have improved signal and improved contrast compared to spiral GRE sequences. Sufficient homogeneity exists at 1.5 T to image 2D slices with a 5.9-ms TR. Nearly optimal moment-nulled spiral rewinder gradients can be calculated analytically and they result in reduced flow artifacts. Spiral trajectories permit the acquisition of 1.8-mm spatial resolution with 118-ms temporal resolution in real time without undersampling. High blood–myocardium contrast is achieved, enabling excellent visualization of blood pool, myocardial wall, and valve leaflet motion.

REFERENCES

1. Yang PC, Kerr AB, Liu AC, Liang DH, Hardy CJ, Meyer CH, Macovski A, Pauly JM, Hu BS. New real-time interactive magnetic resonance imaging complements echocardiography. J Am Coll Cardiol 1998;32:2049–2056.
2. Nayak KS, Pauly JM, Kerr AB, Hu BS, Nishimura DG. Real-time color flow MRI. Magn Reson Med 2000;43:251–258.
3. Yang PC, Meyer C, Terashima M, Kaji S, McConnell MV, Macovski A, Pauly JM, Nishimura DG, Hu BS. Spiral high-resolution magnetic resonance coronary angiography with real-time coronary localization. J Am Coll Cardiol 2003;41:1134–1141.
4. Meyer CH, Hu BS, Nishimura DG, Macovski A. Fast spiral coronary artery imaging. Magn Reson Med 1992;28:202–213.
5. Carr HY. Steady-state free precession in nuclear magnetic resonance. Phys Rev 1958;112:1693–1701.
6. Oppelt A, Graumann R, Barfuss H, Fischer H, Hartl W, Shajor W. FISP—a new fast MRI sequence. Electromedica 1986;54:15–18.
7. Scheffler K, Lehnhardt S. Principles and applications of balanced SSFP techniques. Eur Radiol 2003;13:2409–2418.
8. Simonetti OP, Duerk JL, Chankong V. An optimal design method for magnetic resonance imaging gradient waveforms. IEEE Trans Med Imaging 1993;12:350–360.
9. Hargreaves BA, Nishimura DG, Conolly SM. Time-optimal multi-dimensional gradient waveform design for rapid imaging. Magn Reson Med 2004;51:81–92.
10. Kerr AB, Pauly JM, Hu BS, Li KCP, Hardy CJ, Meyer CH, Macovski A, Nishimura DG. Real-time interactive MRI on a conventional scanner. Magn Reson Med 1997;38:355–367.
11. Nayak KS, Pauly JM, Yang PC, Hu BS, Meyer CH, Nishimura DG. Real-time interactive coronary MRA. Magn Reson Med 2001;46:430–435.
12. Reeder SB, Faranesh AZ, Boxerman JL, McVeigh ER. In vivo measurement of T_2^* and field inhomogeneity maps in the human heart at 1.5 T. Magn Reson Med 1998;39:988–998.
13. Zur Y, Wood ML, Neuringer LJ. Motion-insensitive, steady-state free precession imaging. Magn Reson Med 1990;16:444–459.
14. Nayak KS, Hu BS. Triggered real-time MRI and cardiac applications. Magn Reson Med 2003;49:188–192.
15. Markl M, Alley MT, Elkins CJ, Pelc NJ. Flow effects in balanced steady state free precession imaging. Magn Reson Med 2003;50:892–903.
16. Deimling M, Heid O. Magnetization prepared true FISP imaging. In: Proceedings of the 2nd Annual Meeting of SMR, Dallas, 1994. p 495.
17. Scheffler K, Heid O, Hennig J. Magnetization preparation during the steady-state: fat-saturated 3D true FISP. Magn Reson Med 2001;45:1075–1080.
18. Hargreaves BA, Vasanawala SS, Nayak KS, Hu BS, Nishimura DG. Fat-suppressed steady-state free precession imaging using phase detection. Magn Reson Med 2003;50:210–213.
19. Herzka DA, Kellman P, Aletras AH, Guttman MA, McVeigh ER. Multishot EPI-SSFP in the heart. Magn Reson Med 2002;47:655–664.
20. Slavin GS, Saranathan M. FIESTA-ET: High-resolution cardiac imaging using echo-planar steady-state free precession. Magn Reson Med 2002;48:934–941.